# A dual-emitting mixed-lanthanide MOF with high water-stability for ratiometric fluorescence sensing of $Fe^{3+}$ and ascorbic acid

Haihuan Yu[a], Qun Liu[a], Jiao Li[a], Zhong-Min Su*[b, c, d], Xiao Li*[b, c], Xinlong Wang[b] Jing Sun[b, c], Chen Zhou[b, c], Xiaoli Hu[b, c]

a School of Materials Science and Engineering, Changchun University of Science and Technology, Changchun 130022, People's Republic of China
b School of Chemistry and Environmental Engineering, Changchun University of Science and Technology, Changchun, 130022, People's Republic of China
c Jilin Provincial Science and Technology Innovation Center of Optical Materials and Chemistry, Changchun University of Science and Technology, Changchun, 130022, People's Republic of China
d. Joint Sino-Russian Laboratory of Optical Materials and Chemistry, Changchun 130022, China

* E-mail: zmsu@nenu.edu.cn; lix@cust.edu.cn

## Experimental Procedures

### Materials and Physical Measurements

$Eu(NO_3)_3 \cdot 6H_2O$, $Gd(NO_3)_3 \cdot 6H_2O$, 2,3,5,6-tetrafluoroterephthalic acid ($H_2$tfBDC), 1,10-phenanthroline (phen) and other reagents used in this experiment were purchased and applied directly to the experiments. The C, H, and N elemental analyses were conducted on a PerkinElmer 2400CHN elemental analyzer. Thermogravimetric analysis (TGA) data were obtained with a PerkinElmer TG-7 analyzer in the temperature range of 25-800 °C at a heating rate of 10 °C $min^{-1}$ under a flow of $N_2$. The powders' X-ray diffraction (PXRD) patterns were collected on a Siemens D5005 under experimental conditions with Cu Kα X-ray radiation from $5° < 2\theta < 50°$ at a sweep speed of 0.2 °C × 2θ $min^{-1}$. Fourier transform infrared (FT-IR) spectra were recorded in the range 4000-400 $cm^{-1}$ using KBr pellets on an Alpha Centaurt FT/IR spectrophotometer. The ultraviolet-visible light (UV-vis) absorption spectra were performed on a UV-5500(PC) UV/vis spectrophotometer. Luminescent emission spectra were gained from an F-4500FL fluorescence spectrophotometer. The emission decay traces were recorded on an Edinburgh FLS920 fluorescence spectrophotometer equipped with Xe900, 450W steady state xenon lamp and nanosecond pulse flash lamp, microsecond pulse flash lamp.

### X-ray Collection and Structure Determination

Single-crystal X-ray diffraction data for **Gd-MOF** and **Eu-MOF** were recorded on a Bruker Apex CCD II area-detector diffractometer with graphite monochromated Mo-Kα radiation (λ = 0.71073 Å) at 293(2) K. Absorption corrections were applied using the multi-scan technique. Their structures were solved by the direct methods of SHELXS-97 and refined by the full-matrix least-squares technique with the SHELXL-

97 program.10 Non-hydrogen atoms were refined with anisotropic temperature parameters. The crystal data and structure refinement results of **Eu-MOF** and **Gd-MOF** are summarized in Table S1. The CCDC number of **Eu-MOF and Gd-MOF** are 2008758 and 2008759.

**Table S1.** Crystallographic data for **Eu-MOF, Gd-MOF**.

| | **Eu-MOF** | **Gd-MOF** |
|---|---|---|
| Empirical formula | $C_{24}H_{10}EuF_6N_2O_7$ | $C_{24}H_{10}F_6GdN_2O_7$ |
| Formula weight | 704.30 | 709.59 |
| Temperature/K | 293.15 | 293.15 |
| Crystal system | monoclinic | monoclinic |
| Space group | C2/c | C2/c |
| a/Å | 19.7306(15) | 19.697(9) |
| b/Å | 21.3391(17) | 21.234(9) |
| c/Å | 11.5617(9) | 11.532(6) |
| α/° | 90 | 90 |
| β/° | 102.206(3) | 101.866(16) |
| γ/° | 90 | 90 |
| Volume/Å$^3$ | 4757.8(6) | 4720(4) |
| Z | 8 | 8 |
| $\rho_{calc}$g/cm$^3$ | 1.966 | 1.997 |
| μ/mm$^{-1}$ | 2.734 | 2.908 |
| F(000) | 2728.0 | 2736.0 |
| Crystal size/mm$^3$ | 0.24 × 0.22 × 0.2 | 0.24 × 0.22 × 0.2 |
| Radiation | MoKα (λ = 0.71073) | MoKα (λ = 0.71073) |
| 2Θ range for data collection/ | 5.25 to 50.212 | 5.268 to 50.214 |
| Index ranges | -23 ≤ h ≤ 23, -25 ≤ k ≤ 25, -13 ≤ l ≤ 13 | -23 ≤ h ≤ 23, -25 ≤ k ≤ 25, -13 ≤ l ≤ 13 |
| Reflections collected | 29607 | 27148 |
| Independent reflections | 4251 [$R_{int}$ = 0.0301, $R_{sigma}$ = 0.0175] | 4207 [$R_{int}$ = 0.0918, $R_{sigma}$ = 0.0592] |
| Data/restraints/parameters | 4251/1218/362 | 4207/1231/362 |
| Goodness-of-fit on $F^2$ | 1.062 | 1.016 |
| $R_1$[a] [I>=2σ (I)] | $R_1$ = 0.0347, $wR_2$ = 0.0848 | $R_1$ = 0.0504, $wR_2$ = 0.1137 |
| $wR_2$[b] [all data] | $R_1$ = 0.0433, $wR_2$ = 0.0933 | $R_1$ = 0.0816, $wR_2$ = 0.1291 |
| Largest diff. peak/hole / e Å$^{-3}$ | 1.37/-1.49 | 1.44/-1.63 |

$R_1$[a]= $\Sigma||F_o|-|F_c||/\Sigma|F_o|$, $wR_2$[b] = $[\Sigma[w(F_o^2-F_c^2)^2]/\Sigma[w(F_o^2)^2]]^{1/2}$.

**Table S2** Selected bond distances (Å) for **Eu-MOF**.

| Bond distances (Å) | | | |
|---|---|---|---|
| Eu1-O1[1] | 2.375(3) | Eu1-O5[2] | 2.386(3) |
| Eu1-O2 | 2.376(3) | Eu1-O6 | 2.389(4) |
| Eu1-O3[1] | 2.476(4) | Eu1-N1 | 2.626(4) |
| Eu1-O4[1] | 3.111(4) | Eu1-N2 | 2.575(5) |

Symmetry transformations used to generate equivalent atoms: [1]3/2-X,1/2-Y,1-Z; [2]+X,1-Y,1/2+Z;

[3]1-X,+Y,1/2-Z

**Table S3** Selected angles (º) for **Eu-MOF**.

| Bond angles (˚) | | | |
|---|---|---|---|
| O1[1]-Eu1-O2 | 126.53(13) | O3[1]-Eu1-N1 | 141.55(14) |
| O1[1]-Eu1-O3[1] | 76.24(12) | O3[1]-Eu1-N2 | 149.49(14) |
| O1[1]-Eu1-O4[1] | 66.15(11) | O5[2]-Eu1-O3[1] | 75.76(13) |
| O1[1]-Eu1-O5[2] | 142.82(13) | O5[2]-Eu1-O4[1] | 107.79(12) |
| O1[1]-Eu1-O6 | 77.18(13) | O5[2]-Eu1-O6 | 73.37(13) |
| O1[1]-Eu1-N1 | 74.30(14) | O5[2]-Eu1-N1 | 116.23(14) |
| O1[1]-Eu1-N2 | 134.06(14) | O5[2]-Eu1-N2 | 75.29(14) |
| O2-Eu1-O3[1] | 83.83(13) | O6-Eu1-O3[1] | 77.73(14) |
| O2-Eu1-O4[1] | 64.90(11) | O6-Eu1-O4[1] | 116.13(13) |
| O2-Eu1-O5[2] | 73.69(13) | O6-Eu1-N1 | 72.09(14) |
| O2-Eu1-O6 | 145.27(13) | O6-Eu1-N2 | 102.82(15) |
| O2-Eu1-N1 | 133.99(14) | N1-Eu1-O4[1] | 135.37(12) |
| O2-Eu1-N2 | 79.03(14) | N2-Eu1-O4[1] | 140.32(13) |
| O3[1]-Eu1-O4[1] | 44.66(11) | N2-Eu1-N1 | 62.71(15) |

Symmetry transformations used to generate equivalent atoms: [1]3/2-X,1/2-Y,1-Z; [2]+X,1-Y,1/2+Z; [3]+X,1-Y,-1/2+Z; [4]1-X,+Y,1/2-Z

**Table S4** Selected bond distances (Å) and angles (º) for **Gd-MOF**.

| Bond distances (Å) | | | |
|---|---|---|---|
| Gd1-O1 | 2.337(6) | Gd1-O5[1] | 2.458(6) |
| Gd1-O2 | 2.356(6) | Gd1-N1 | 2.608(7) |
| Gd1-O3[1] | 2.423(6) | Gd1-O6 | 2.372(6) |
| Gd1-O4[2] | 2.431(6) | Gd1-N2 | 2.561(8) |

Symmetry transformations used to generate equivalent atoms: [1]3/2-X,1/2-Y, 1-Z; [2]3/2-X,-1/2+Y, 3/2-Z; [3]1-X,+Y,1/2-Z

| Bond angles (˚) | | | |
|---|---|---|---|
| O1-Gd1-O2 | 74.9(2) | O3[1]-Gd1-O5[1] | 83.4(2) |
| O1-Gd1-O3[1] | 74.5(2) | O3[1]-Gd1-N1 | 134.4(2) |
| O1-Gd1-O4[2] | 141.5(2) | O3[1]-Gd1-N2 | 79.3(2) |
| O1-Gd1-O5[1] | 120.7(2) | O4[2]-Gd1-O5[1] | 75.7(2) |
| O1-Gd1-N1 | 73.6(2) | O4[2]-Gd1-N1 | 116.8(2) |
| O1-Gd1-O6 | 140.6(2) | O4[2]-Gd1-N2 | 75.6(2) |
| O1-Gd1-N2 | 78.1(2) | O5[1]-Gd1-N1 | 141.4(2) |
| O2-Gd1-O3[1] | 125.9(2) | O5[1]-Gd1-N2 | 149.7(2) |
| O2-Gd1-O4[2] | 142.6(2) | O6-Gd1-O3[1] | 144.9(2) |
| O2-Gd1-O5[1] | 75.5(2) | O6-Gd1-O4[2] | 73.2(2) |
| O2-Gd1-N1 | 74.6(2) | O6-Gd1-O5[1] | 78.1(2) |
| O2-Gd1-O6 | 77.8(2) | O6-Gd1-N1 | 72.1(2) |
| O2-Gd1-N2 | 134.6(2) | O6-Gd1-N2 | 102.6(3) |
| O3[1]-Gd1-O4[2] | 73.5(2) | N1-Gd1-N2 | 63.0(2) |

Symmetry transformations used to generate equivalent atoms: [1]3/2-X,1/2-Y,1-Z; [2]3/2-X,-1/2+Y,3/2-Z; [3]3/2-X,1/2+Y,3/2-Z; [4]1-X,+Y,1/2-Z

**Table S5.** The molar ratio of Eu/Gd in compounds produced by ICP.

| Sample | The molar of the starting Eu/Gd salt | The molar by ICP analysis |
|---|---|---|
| $Eu_{0.03}Gd_{0.07}$-MOF | 0.03:0.07 | 0.0311:0.068 |
| $Eu_{0.04}Gd_{0.06}$-MOF | 0.04:0.06 | 0.0436:0.061 |
| $Eu_{0.05}Gd_{0.05}$-MOF | 0.05:0.05 | 0.0526:0.054 |
| $Eu_{0.06}Gd_{0.04}$-MOF | 0.06:0.04 | 0.0635:0.037 |
| $Eu_{0.07}Gd_{0.03}$-MOF | 0.07:0.03 | 0.0719:0.028 |
| $Eu_{0.08}Gd_{0.02}$-MOF | 0.08:0.02 | 0.0827:0.019 |
| $Eu_{0.09}Gd_{0.01}$-MOF | 0.09:0.01 | 0.0911:0.009 |

**Table S6.** Comparison the LOD of **$Eu_{0.07}Gd_{0.03}$-MOF** towards $Fe^{3+}$ with other materials.

| Materials | analytes | LOD (μM) | Ref. |
|---|---|---|---|
| $Eu_{0.07}Gd_{0.03}$-MOF | $Fe^{3+}$ | 0.091 | This work |
| RhB@DiCH$_3$MOF-5 | $Fe^{3+}$ | 0.36 | [1] |
| $\{[Tb(Cmdcp)(H_2O)_3]_2(NO_3)_2\cdot 5H_2O\}_n$ | $Fe^{3+}$ | 0.40 | [2] |
| $\{(Me_2NH_2)[Tb(OBA)_2]\cdot(Hatz)\cdot(H_2O)_{1.5}\}_n$ | $Fe^{3+}$ | 0.10 | [3] |
| Tb-MOF-A | $Fe^{3+}$ | 0.13 | [4] |
| $[Eu(Hmcd)(H_2O)(DMF)_2]_n$ | $Fe^{3+}$ | 0.095 | [5] |
| $[L_4Cd_3(H_2O)_2]_n$ | $Fe^{3+}$ | 0.095 | [6] |
| ZJU109 | $Fe^{3+}$ | 0.53 | [7] |

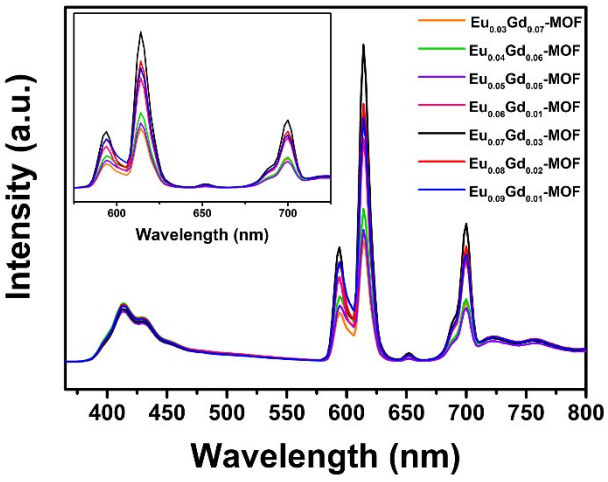


**Figure S1** The emission spectra of **$Eu_xGd_{0.1-x}$-MOF**.

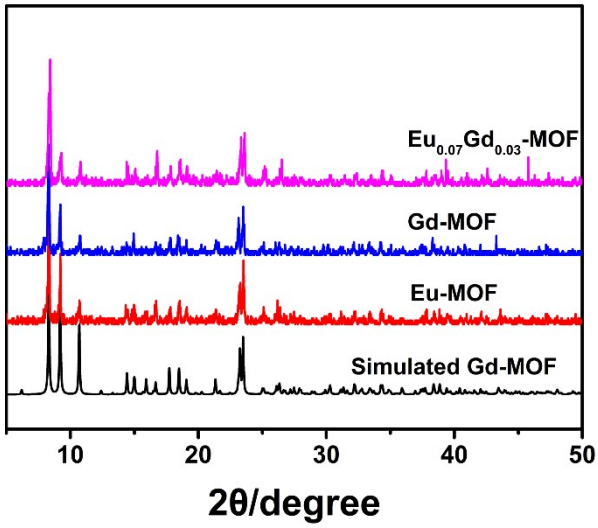


**Figure S2** Simulated and experimental powder X-ray diffraction patterns (PXRD) of **Eu-MOF, Gd-MOF, $Eu_{0.07}Gd_{0.03}$-MOF**.

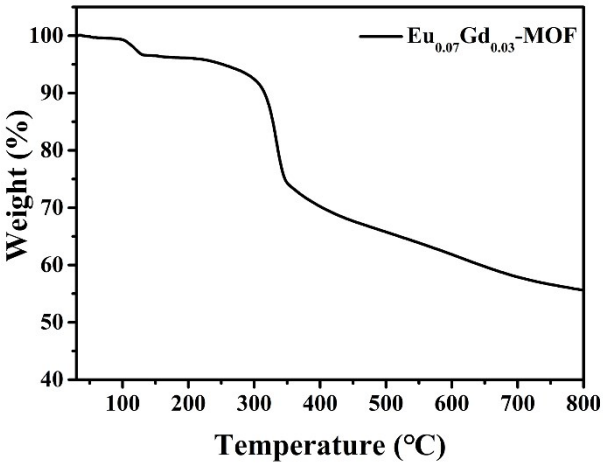


**Figure S3** TGA curve of **$Eu_{0.07}Gd_{0.03}$-MOF**.

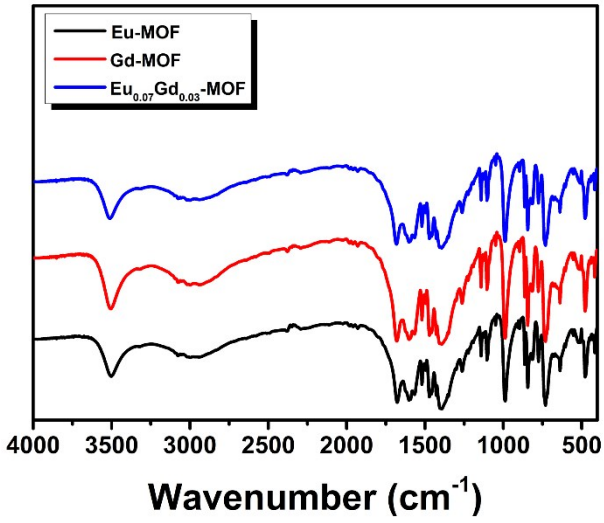


**Figure S4** FTIR spectra of **Eu-MOF, Gd-MOF, $Eu_{0.07}Gd_{0.03}$-MOF**.

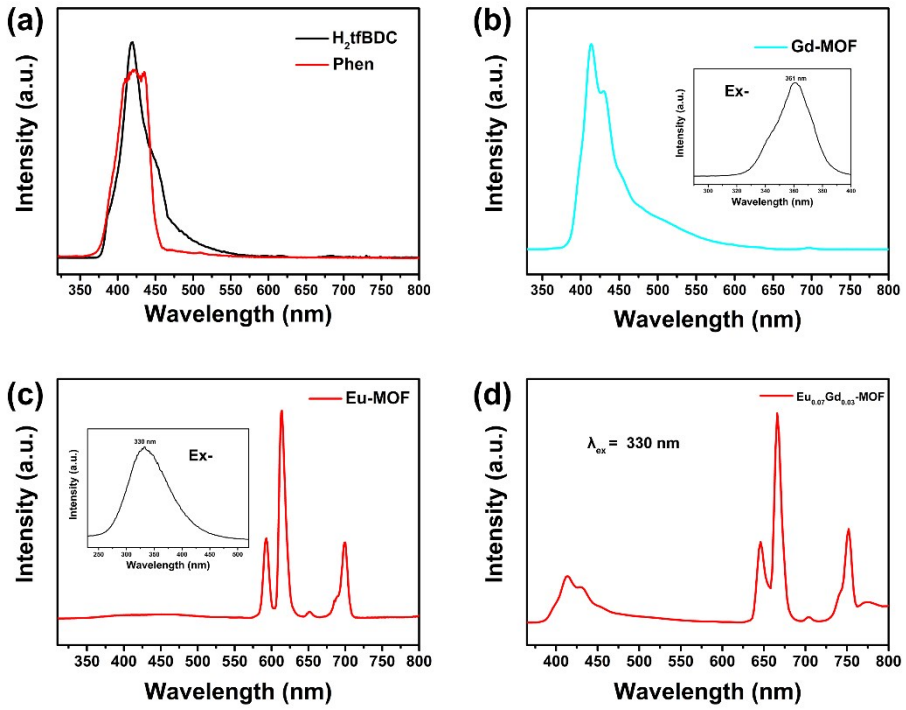


**Figure S5** Solid luminescence spectra of ligands, **Gd-MOF**, **Eu-MOF, $Eu_{0.07}Gd_{0.03}$-MOF**.

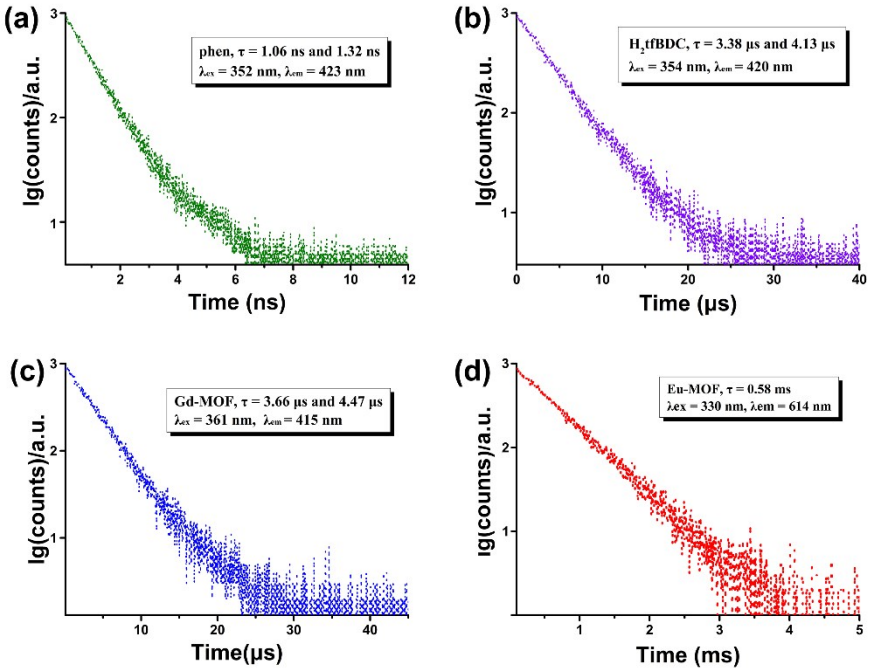


**Figure S6** The luminescent lifetime decay curves of Phen ligand, $H_2$tfBDC ligand, Gd-MOF and Eu-MOF

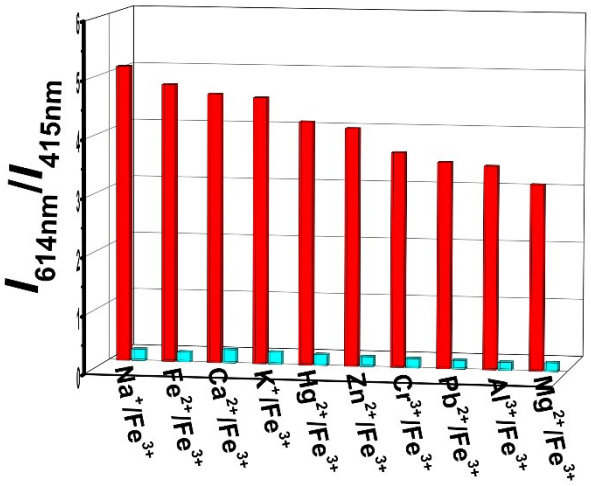


**Figure S7** Fluorescence response of the **$Eu_{0.07}Gd_{0.03}$-MOF** to $Fe^{3+}$ and other metal ions exist in water (500 μM).

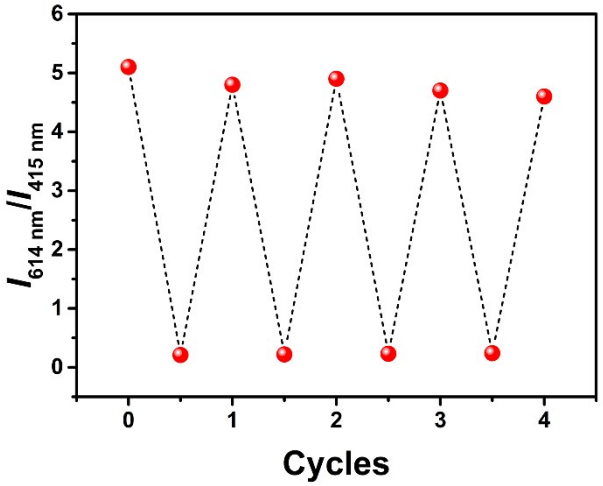


**Figure S8** Fluorescence quenching and enhancement cycles of the $I_{614nm}/I_{415nm}$ upon the **$Eu_{0.07}Gd_{0.03}$-MOF** dipping in 500 μM $Fe^{3+}$.

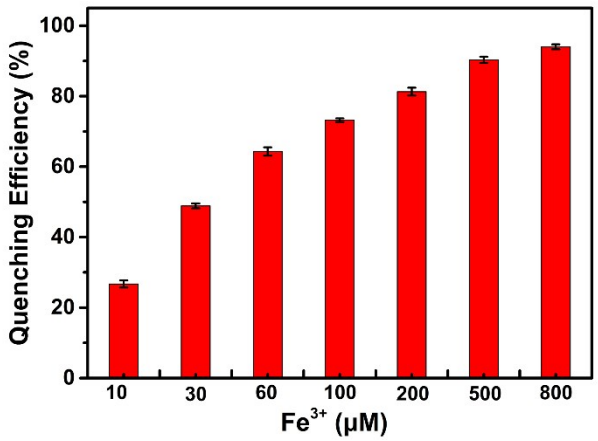


**Figure S9** The $Eu^{3+}$-based quenching efficiency of **$Eu_{0.07}Gd_{0.03}$-MOF** (3 mg) to various concentrations of $Fe^{3+}$.

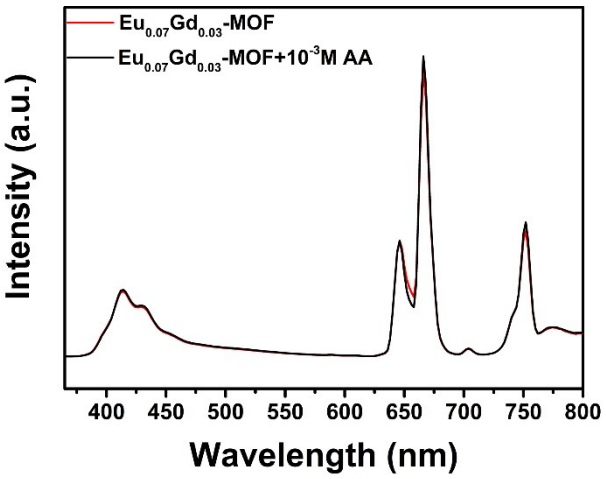


**Figure S10** Fluorescence spectra of **$Eu_{0.07}Gd_{0.03}$-MOF** and **$Eu_{0.07}Gd_{0.03}$-MOF** with ascorbic acid.

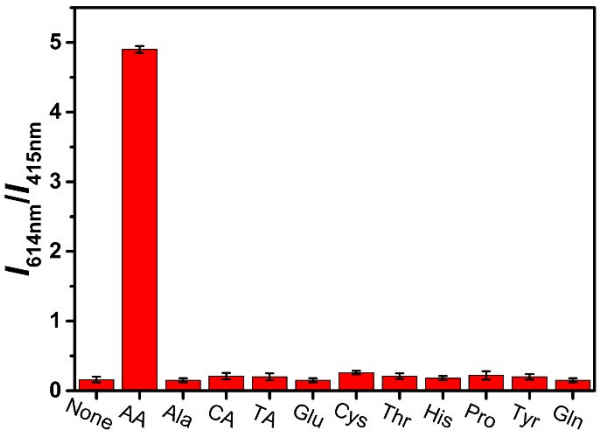


**Figure S11** Responses of **$Eu_{0.07}Gd_{0.03}$-MOF/ $Fe^{3+}$** towards other interfering substances (500 μM).

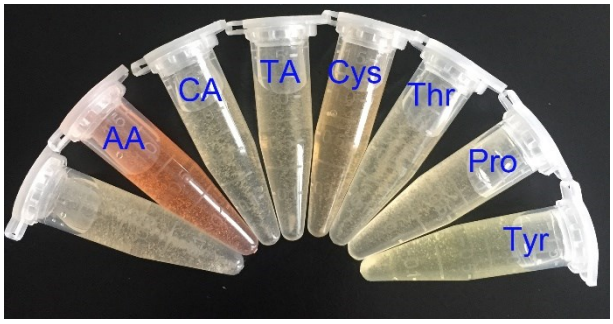


**Figure S12**A photograph of **$Eu_{0.07}Gd_{0.03}$-MOF/$Fe^{3+}$**, **$Eu_{0.07}Gd_{0.03}$-MOF/$Fe^{3+}$** + ascorbic acid (500 μM), **$Eu_{0.07}Gd_{0.03}$-MOF/$Fe^{3+}$** + other interfering substances (500 μM): in the presence of 1,10-phenanthroline under visual light, respectively.

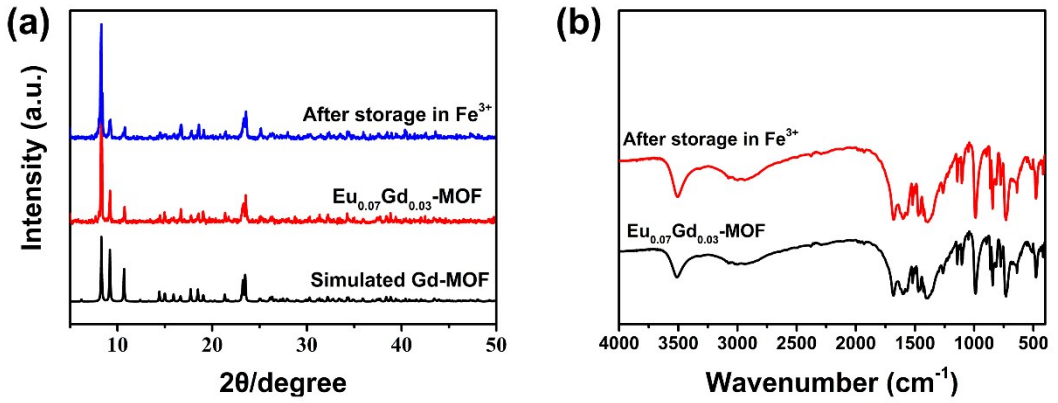


**Figure S13** PXRD patterns and IR spectra of **$Eu_{0.07}Gd_{0.03}$-MOF** after storage in $Fe^{3+}$ aqueous solutions.

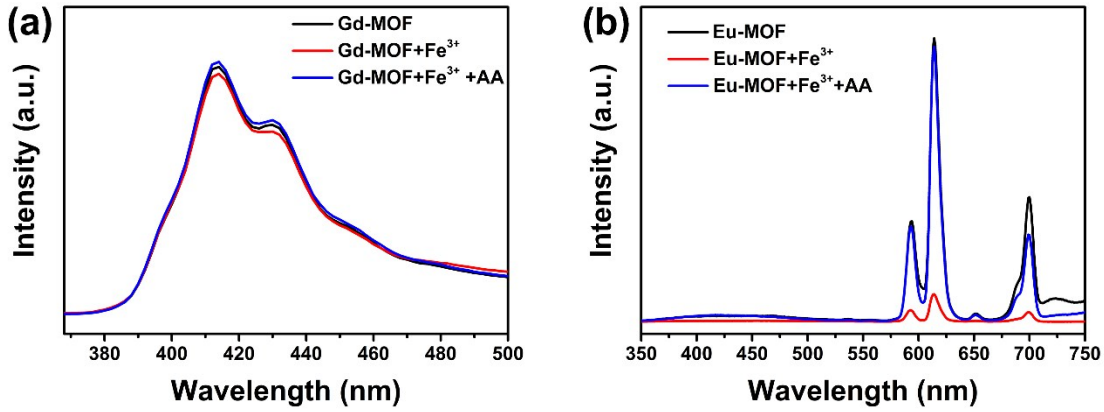


**Figure S14** Emission spectra of the **Gd-MOF** and **Eu-MOF**, **Gd-MOF** and **Eu-MOF** after storage in $Fe^{3+}$ aqueous solutions (500 μM) and **Gd-MOF/$Fe^{3+}$** and **Eu-MOF/$Fe^{3+}$** after storage in AA (500 μM).

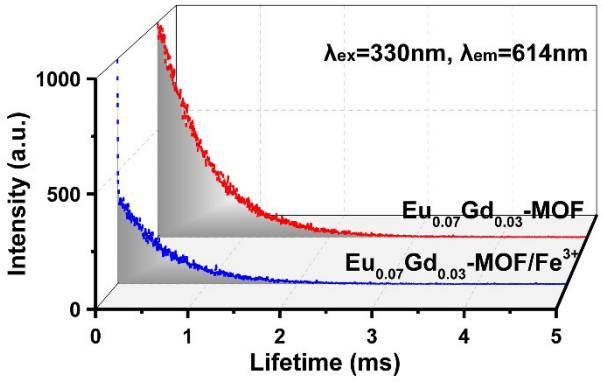


**Figure S15** The luminescence decay curves of $^5D_0 \rightarrow {}^7F_2$ ($Eu^{3+}$) in $Eu_{0.07}Gd_{0.03}$-MOFs and $Eu_{0.07}Gd_{0.03}$-MOFs/$Fe^{3+}$

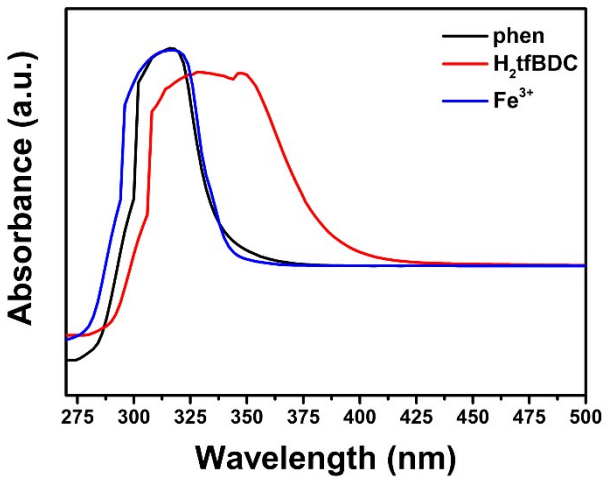


**Figure S16** Spectral overlap between absorption spectra of the ligands phen, $H_2$tfBDC and $Fe^{3+}$in water.

## References

[1] L. Guo, Y. Liu, R. M Kong, G. Chen, Z. Liu, F. L. Qu, L. Xia and W. H. Tan, A Metal-Organic Framework as Selectivity Regulator for $Fe^{3+}$ and Ascorbic Acid Detection, *Anal. Chem.,* 2019, **91**, 12453-12460.

[2] K. Y. Wu, L. Qin, C. Fan, S. L. Cai, T. T. Zhang, W. H Chen, X. Y. Tang and J. X. Chen, Sequential and recyclable sensing of $Fe^{3+}$ and ascorbic acid in water with a terbium(III)-based metal–organic framework, *Dalton Trans.,* 2019, **48**, 8911-8919.

[3] D. M. Chen, N. N. Zhang, C. S. Liu and M. Du, Template-directed synthesis of a luminescent Tb-MOF material for highly selective $Fe^{3+}$ and $Al^{3+}$ ions detection and VOC vapor sensing. *J. Mater. Chem. C,* 2017, **5** , 2311-2317.

[4] H. Yu, J. Chi, Z. Su, X. Li, J. Sun, C. Zhou, X. Hu and Q. Liu, A water-stable terbium metal-organic framework with functionalized ligands for the detection of $Fe^{3+}$, $Cr_2O_7^{2-}$ ions in water and picric acid in seawater, *CrystEngComm,* 2020, **22**, 3638-3643.

[5] X, Li, J, Tang, H, Liu, K, Gao, X, Meng, J, Wu and H. Ho, High Sensitive and Recyclable Ln-MOF Luminescent Sensor for Efficient Detection of $Fe^{3+}$, $Cr^{VI}$ Anions with Carbazolyl-tetracarboxylate Ligand, *Chem. Asian J.,* 2019, **14**, 3721-3727.

[6] K. Wu, J. Hu, S. Shi, J. Li, X. Cheng, A thermal stable pincer-MOF with high selective and sensitive nitro explosive TNP, metal ion $Fe^{3+}$ and pH sensing in aqueous solution, *Dyes and Pigments,* 2020, **173**, 107993.

[7] Y. J. Cui, D. Yue, Y. K. Huang, J. Zhang, Z. Y. Wang, D. R. Yang and G. D. Qian, Photo-Induced Electron Transfer in Metal-Organic Framework: A new Approach Towards highly sensitive luminescent probe of $Fe^{3+}$, *Chem. Commun.,* 2019, **55**, 11231-11234.